JOURNAL OF VIROLOGY, Aug. 2005, p. 9470–9479 Vol. 79, No. 15
0022-538X/05/$08.00+0 doi:10.1128/JVI.79.15.9470–9479.2005

Apical Entry and Release of Severe Acute Respiratory Syndrome-Associated Coronavirus in Polarized Calu-3 Lung Epithelial Cells

Chien-Te K. Tseng,[1,2]* Jennifer Tseng,[2] Lucy Perrone,[2] Melissa Worthy,[1] Vsevolod Popov,[2] and Clarence J. Peters[1,2]

Department of Microbiology and Immunology,[1] and Department of Pathology,[2] University of Texas Medical Branch, Galveston, Texas 77555-0609

Received 5 January 2005/Accepted 14 April 2005

Severe acute respiratory syndrome (SARS), caused by a novel coronavirus (CoV) known as SARS-CoV, is a contagious and life-threatening respiratory illness with pneumocytes as its main target. A full understanding of how SARS-CoV would interact with lung epithelial cells will be vital for advancing our knowledge of SARS pathogenesis. However, an in vitro model of SARS-CoV infection using relevant lung epithelial cells is not yet available, making it difficult to dissect the pathogenesis of SARS-CoV in the lungs. Here, we report that SARS-CoV can productively infect human bronchial epithelial Calu-3 cells, causing cytopathic effects, a process reflective of its natural course of infection in the lungs. Indirect immunofluorescence studies revealed a preferential expression of angiotensin-converting enzyme 2 (ACE-2), the functional receptor of SARS-CoV, on the apical surface. Importantly, both ACE-2 and viral antigen appeared to preferentially colocalize at the apical domain of infected cells. In highly polarized Calu-3 cells grown on the membrane inserts, we found that cells exposed to virus through the apical rather than the basolateral surface showed high levels of viral replication. Progeny virus was released into the apical chamber at titers up to 5 logs higher than those recovered from the basolateral chambers of polarized cultures. Taken together, these results indicate that SARS-CoV almost exclusively entered and was released from the apical domain of polarized Calu-3 cells, which might provide important insight into the mechanism of transmission and pathogenesis of SARS-CoV.

Severe acute respiratory syndrome (SARS) originated in Guangdong, China, in late 2002 and emerged by early 2003 as a highly contagious and life-threatening pulmonary illness, causing a devastating social, economic, and medical impact worldwide (4, 29). As of July 2003, this atypical pneumonic disease had affected more than 8,000 people in 28 regions, with a case fatality rate of 9.6% (34). The causative agent of SARS has been identified as a distinct coronavirus (CoV), now known as SARS-CoV (8, 15, 24).

The outcome of virus-cell interactions depends on many factors of both viral and cellular origin. SARS-CoV is transmitted primarily by virus-laden droplets and possibly also via the aerosol or fecal-oral routes, with the lung epithelial cells and intestinal epithelial cells as the primary targets for its replication (6, 15, 23). Pathological studies in autopsy and biopsy samples of SARS patients revealed few microscopic lesions in the intestinal epithelial linings of the gastrointestinal tract, despite its being the only extrapulmonary site where infectious SARS-CoV could be readily identified (6, 19, 30). This pathology-resistant trait of intestinal epithelial cells observed in SARS patients has recently been extended to include ex vivo models in which SARS-CoV was shown to persistently infect human intestinal epithelial cell lines (e.g., Caco-2 and LoVo) without causing any cytopathic effects (CPE) (5, 21). In contrast, most SARS-associated clinical and pathological manifestations, with the exception of diarrhea, have involved the respiratory system, causing extensive pulmonary consolidation and diffuse alveolar damage of varying severity in severely affected patients (7, 10, 17–19, 23, 29, 35). The pathogenesis of SARS-CoV infection in the lungs remains unknown, largely due to the absence of an ex vivo culture system that reflects the natural course of respiratory infection.

Viral pathogenesis is known to begin with virus interaction with host cells. Entry of SARS-CoV into permissive cells, like other human and animal CoVs, is mediated through the binding of its spike (S) envelope protein to corresponding cellular receptors (12, 27). Thus, the differential expression of angiotensin-converting enzyme 2 (ACE-2), a functional cellular receptor for SARS-CoV (20, 33), could contribute to the pathogenesis of SARS. Indeed, ACE-2 has been shown to be abundantly expressed on the surface of lung and intestinal epithelial cells, consistent with their susceptibility to SARS-CoV (11). Additionally, epithelial cells are highly polarized cells with two compositionally distinct membrane domains, namely, the apical and basolateral domains, which are separated by specialized molecular complexes, termed tight junctions (13). Preferential interactions of viruses with polarized epithelial cells through apical or basolateral surfaces, with regard to viral binding, internalization, and release, would have important implications for viral pathogenesis. Thus, the polarity of entry into and release from polarized epithelium has been studied extensively with various viruses. For instance, Sendai virus, respiratory syncytial virus, and human CoV 229E have been shown to preferentially enter through and release

* Corresponding author. Mailing address: Department of Microbiology and Immunology, University of Texas Medical Branch, 301 University Boulevard, G-150 Keiller Building, Galveston, TX 77555-0609. Phone: (409) 772-0091. Fax: (409) 747-0762. E-mail: sktseng@utmb.edu.

from the apical surface, whereas measles virus enters the epithelial cells from the apical domain and is released from both the apical and basolateral surfaces (25, 28, 32). Since lung epithelial cells of the respiratory tract are considered the initial target for SARS-CoV replication, a full understanding of how SARS-CoV would interact with these polarized lung epithelial cells is crucial for advancing our knowledge of SARS pathogenesis. Unfortunately, no human respiratory epithelial cell lines have been shown as yet to support SARS-CoV infection.

Here, we report that a continuous human lung epithelial cell line, Calu-3, is highly permissive for SARS-CoV infection, as evidenced by quantitation of infectious viral particles, detection of viral antigens, and visualized viral particles. In contrast to its null effect on permissive human intestinal epithelial Caco-2 or LoVo cells, SARS-CoV induced CPE in Calu-3 cells, mimicking the natural course of infection in the lungs. As an initial step toward understanding the pathogenesis of SARS, we also studied the polarity of SARS-CoV infection and the expression of ACE-2 in Calu-3 cells. We found that ACE-2 is preferentially expressed at the apical domain of polarized Calu-3 cells and that infection and release of SARS-CoV are almost exclusively mediated through the apical surface. This apical-surface-to-apical-surface spread of SARS-CoV in lung epithelial cells, as revealed by our results, would provide important insight into both the respiratory route of viral transmission and the pathogenesis of SARS-CoV in the lungs.

MATERIALS AND METHODS

Cells. Vero E6 cells were grown in Dulbecco's modified Eagle's minimal essential medium (DMEM) supplemented with 10% fetal bovine serum, designated D-10 medium, whereas human lung epithelial Calu-3 cells (American Type Culture Collection), a generous gift from Tonyia Eaves-Pyles, University of Texas Medical Branch (UTMB), were grown in DMEM medium supplemented with 20% fetal calf serum (FCS) (D-20) medium. Calu-3 cells, which originated from a human pulmonary adenocarcinoma, have been well characterized as nonciliated human lung/bronchial epithelial cells with a mixed phenotype and have been used in many areas of biomedical research since their establishment. Specifically, Calu-3 cells do not express 15-lipooxygenase, an enzyme specifically localized at the surface epithelium; however, they do express other markers of serous gland cells, including secretory component, secretory leukocyte protease inhibitor, lysozyme, lactoferrin, and cystic fibrosis transmembrane conductance regulator (1, 9, 26). In addition to the serous phenotype, Calu-3 cells express the mucine gene *muc-2*, which is usually expressed on the surface of goblet and gland mucous cells of native airway epithelial cells (9). We also noticed that approximately 10 to 15% of Calu-3 cells in the confluent cultures contained electron-lucent secretory granules (data not shown) resembling those of goblet or mucous gland cells of the airway epithelium, as described previously (26). Taken together, Calu-3 cells are likely derived from the submucosal gland serous cells. For studies of ACE-2 and viral antigen expression and the polarity of virus entry and release, Calu-3 cells were grown on 4-well chamber slides (Lab-Tek, catalog no. 177399; Nalge Nunc International, Naperville, IL) and on collagen-coated, semipermeable membranes with a 0.4-μm pore size (Transwell, catalog no. 3470-clear; Corning Inc., Corning, NY), respectively. The cells were seeded at 10^6 cells per chamber or filter, and the medium was changed every 2 to 3 days. Confluent cultures of Calu-3 cells usually consisted of a single layer of cells with irregular depth. Highly polarized Calu-3 monolayers (usually greater than 10 days postconfluence), as evidenced by the formation of tight junctions between adjacent cells and the visualization of microvilli at the apical surface using transmission electromicroscopy (TEM), as shown in Fig. 10, were used in the polarity studies.

Virus and titration of virus. The Urbani strain of SARS-CoV, kindly provided to us by T. G. Ksiazek, Centers for Disease Control and Prevention, Atlanta, Ga., was used throughout this study. The original stock of SARS-CoV (passage 2 in Vero E6 cells) was subjected to two additional passages in Vero E6 cells. A cell-free viral stock with a titer of 1×10^7 50% tissue culture infectious doses ($TCID_{50}$)/ml was generated and stored at −80°C. Some aliquots of this infectious stock were irradiated (2×10^6 rads from a cobalt^{60} source), according to a predetermined kill curve, and used as γ-inactivated SARS-CoV in these studies. All experiments involving infectious viruses were conducted in an approved biosafety level 3 laboratory at UTMB.

The infectious viral titers in the cell-free supernatants collected at different time points postinfection were determined by a standard $TCID_{50}$ assay on permissive Vero E6 cell monolayers in 24-well plates with a series of 10-fold-diluted samples. The titer of individual samples was expressed as $TCID_{50}$ per milliliter of sample.

RT-PCRs for quantifying subgenomic mRNA 5 (M protein) of SARS-CoV. Total RNA was isolated from γ-inactivated or live SARS-CoV-infected Calu-3 cells at the indicated time points after infection by a standard protocol using TRIzol reagent (Invitrogen Life Technologies, Carlsbad, CA). Contaminating genomic DNA was digested with DNase I during the extraction procedure. The primer pair and probe for detecting SARS-CoV-specific subgenomic mRNA 5 (M protein) were as follows: primer forward (5′-AGGTTTCCTATTCCTAGC CTGGATT), primer reverse (5′-AGAGCCAGAGGAAAACAAGCTTTAT), and the sequence ACCTGTTCCGATTAGAATAG as a detection probe, all of which were derived by using Assays-by-design (P/N4331348) (Applied Biosystems). The predeveloped primer set and TaqMan probe for 18S rRNA (P/N4319413E) were used as the endogenous control. One-step real-time PCR (RT-PCR) was used to quantify the expression of SARS-CoV-specific subgenomic mRNA 5 sequences at the indicated time points after infection. Briefly, 0.5 μg RNA was transferred to separate tubes for amplifying the target gene (SARS-CoV) and endogenous control (18S rRNA), respectively, by using a TaqMan one-step RT-PCR master mix reagent kit (P/N4309169). The cycling parameters for one-step RT-PCR were as follows: reverse transcription at 48°C for 30 min, AmpliTaq activation at 95°C for 10 min, denaturation at 95°C for 15 s, and annealing/extension at 60°C for 1 min. A total of 40 cycles were performed on an ABI PRISM 7000 real-time thermocycler (Applied Biosystems), according to the manufacturer's instructions. DNA fragments encoding SARS-CoV-specific subgenomic mRNA 5 were amplified in triplicate with 18S rRNA, and relative mRNA levels for each sample were calculated as follows: Δ cycle threshold (C_t) = C_t SARS-CoV − C_t 18S rRNA; ratio (mRNA in infected cells/mRNA in mock-infected cells) = $2^{-(\Delta Ct \text{ infected} - \Delta Ct \text{ mock})}$.

Immunofluorescence staining and confocal microscopy. Uninfected and SARS-CoV-infected (multiplicity of infection [MOI] = 1) Calu-3 cells grown on the chamber slides were washed with phosphate-buffered saline (PBS), fixed in 2% paraformaldehyde overnight, and rinsed with PBS. After blocking with PBS containing 5% bovine serum albumin for 30 min, fixed Calu-3 monolayers were incubated for 1 h at 37°C with one of the following primary antibodies: goat anti-human ACE-2 (5 μg/ml; R&D system), human convalescent-phase serum against SARS-CoV (1:2,000 dilution), or rabbit anti-SARS-CoV nucleocapsid protein (NP) (IG-549 [2 μg/ml]; IMGENEX). After washing, cells were stained with diluted (1:100) fluorescein isothiocyanate (FITC)- or Texas red-conjugated rabbit anti-human immunoglobulin G (IgG) (Santa Cruz Biotechnology, Inc., Santa Cruz, CA) or donkey anti-goat IgG (Molecular Probes, Eugene, OR) at 37°C for an hour. Normal human and rabbit sera were included as controls for the primary antibodies. Cells were counterstained with antifade reagent containing DAPI (4′,6′-diamidino-2-phenylindole) (Molecular Probes). Fluorescent images were captured with conventional UV microscopy or a laser scanning confocal microscope (Zeiss LSM 510; Optical Imaging Core facility at UTMB).

Infection of Calu-3 cells. Confluent Calu-3 cell cultures grown in flasks, chamber slides, or 24-well plates were infected with SARS-CoV at indicated MOIs by using standard protocols. In some experiments, Calu-3 cell cultures were pretreated with goat anti-human ACE-2 antibody (catalog no. AF933; R&D Systems) or irrelevant goat antibody for assessing the role of ACE-2 in SARS-CoV replication. For determining the polarity of viral entry and release, postconfluent (14 to 17 days) monolayers of Calu-3 cells grown in the transwell inserts were infected with SARS-CoV (MOI = 1) through the apical surface by directly applying infectious viruses (100 μl) to the apical chambers of the transwell culture system. To infect through the basolateral surface, the membrane inserts containing polarized Calu-3 cells were turned over and the viruses were applied to the basolateral surface. Following a 2-h incubation, the unbound viruses were washed off with PBS and the basolaterally infected inserts were turned upright and allowed to incubate for an additional 48 h. Supernatants were obtained from both the apical and the basolateral chambers for viral titration, whereas inserts were processed for visualization of viral particles by TEM.

Transmission electron microscopy. Highly polarized Calu-3 cells on the membrane inserts were infected with SARS-CoV at an MOI of 2. At 48 h after infection, cells were washed with PBS and fixed in a mixture of 2.5% formaldehyde, 0.1% glutaraldehyde, 0.03% trinitrophenol, and 0.03% $CaCl_2$ in 0.05 M

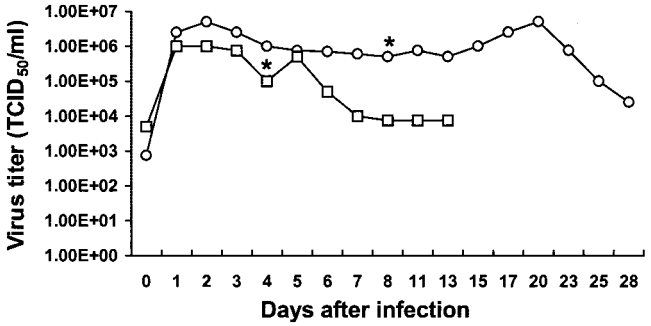

FIG. 1. Kinetics of SARS-CoV replication in infected human lung epithelial Calu-3 cells. Calu-3 cells were infected with SARS-CoV at an MOI of 1 for 1 h at 37°C. After washing (twice) to remove unbound viral particles, infected Calu-3 cells were cultured in medium containing 20% (○) or 2% (□) FCS and observed daily for CPE. One milliliter of cell-free supernatant was harvested at the indicated time points after infection, accompanied by replenishment with 1 ml of fresh medium. Supernatants were kept frozen at −80°C until they were needed for assessing infectious viral titers by a standard $TCID_{50}$ assay with permissive Vero E6 cells, as described in Materials and Methods. Asterisks (*) indicate the time when CPE was first observed. The growth curve of SARS-CoV in Calu-3 cells was representative of two independently conducted experiments.

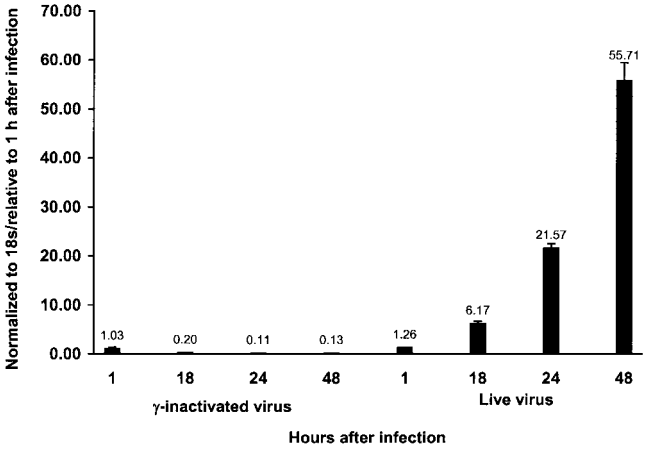

FIG. 2. Assessment of SARS-CoV replication by quantitative RT-PCR. Calu-3 cells were harvested at 1, 18, 24, and 48 h after infection with γ-inactivated or live SARS-CoV at an MOI of 1. Total RNA was extracted and subjected to quantitative RT-PCR for amplification of virus-specific subgenomic mRNA 5 (M protein) species. The intensity of mRNA 5 expression was normalized to 18S RNA. The average of mRNA signals in duplicated samples is depicted.

cacodylate buffer, pH 7.2, added to the well to cover the membrane from both sides. After washing in 0.1 M cacodylate buffer, the cells were postfixed in 1% OsO_4 in the same buffer, stained en bloc in 1% uranyl acetate in 0.1 M maleate buffer, pH 5.2, dehydrated in ethanol, and embedded in Poly/Bed 812 (Polysciences, Warrington, PA). Before embedding, membranes were cut out, sliced into stripes, and stacked at one side of a flat embedding mold. Semithin sections were cut first, stained with toluidine blue, and examined to choose the areas of confluent monolayers for ultrathin sectioning. Ultrathin sections were cut with a Leica-Reichert Ultracut S ultramicrotome, stained with 2% aqueous uranyl acetate and lead citrate, and examined with a Philips 201 or CM-100 electron microscope at 60 kV.

RESULTS AND DISCUSSION

SARS-CoV productively infects human bronchial epithelial cells, causing CPE. In the course of searching for a relevant cell culture model for SARS-CoV replication, we infected an established cell line of human bronchial epithelial origin, Calu-3. Monolayers of Calu-3 cells were inoculated with SARS-CoV at an MOI of 0.1. To determine whether they were susceptible to SARS-CoV infection, the titers of infectious viral particles in the supernatants harvested at indicated time points after infection were assessed. Because Calu-3 cells were grown in a medium containing 20% FCS, virally infected cells were also tested in this medium and the usual 2% FCS medium. As shown in Fig. 1, a representative of two independent experiments, minimum 100- and 1,000-fold increases in the yields of infectious viral particles were consistently observed within 24 h in infected Calu-3 cells maintained in medium supplemented with 2% and 20% heat-inactivated FCS, respectively. Although the viral yields reached a maximum at days 1 and 2 after infection, depending upon the serum content in the culture medium, the infectivity of supernatants harvested thereafter without further passage of infected cells remained prominent.

To further verify the permissiveness of Calu-3 cells to SARS-CoV, we analyzed the expression of subgenomic mRNA 5 (M protein) at different time points after infection by quantitative real-time PCRs. As shown in Fig. 2, a dramatic increase in the expression of mRNA 5 could be readily detected in Calu-3 cells within 24 to 48 h after infection, confirming viral replication in Calu-3 cells. Indirect immunofluorescence staining with confocal imaging using convalescent-phase serum from a SARS patient also demonstrated the expression of SARS-CoV-specific antigens in some, but not all, areas of infected Calu-3 monolayers at day 2 after infection (Fig. 3).

SARS-CoV lytically infects Vero E6 cells, resulting in profound CPE with characteristic cell rounding. However, it persistently infects permissive human intestinal epithelial cell lines, such as Caco-2 and LoVo, without causing any CPE (5, 21). Thus, we also investigated the nature of productive SARS-CoV infection in Calu-3 cells by examining microscopic lesions of infected cells cultured in medium supplemented with either 2% or 20% FCS. As with Vero E6 cells, SARS-CoV infection induced CPE in Calu-3 cells. However, in contrast to Vero E6 cells, where CPE usually occurred within 24 to 36 h after infection, coincident with the maximal release of infectious viral particles (21, 22), no visible CPE could be observed until day 4 or 8 in infected Calu-3 cells, depending on the serum content in the culture medium. Additionally, the morphology of CPE in infected Calu-3 cultures was considerably different from that observed in Vero E6 cells (7, 21–23, 30). Specifically, elongated or balloon-like cells, eventually followed by the cellular detachment in the absence of cellular fusion as shown in Fig. 4, appear to be a characteristic feature of SARS-CoV-associated CPE in Calu-3 monolayers. The cell detachment of infected Calu-3 cells cultured in 20% FCS-containing medium starting from day 8 eventually reached over 95% of the monolayers by day 28 after infection. Interestingly, when cultured in medium containing 2% rather than 20% FCS, more than 95% of infected Calu-3 monolayers were detached at day 14 (data not shown), suggesting that the kinetics of CPE progression are also dependent on the serum content in the medium. Although the factors and mechanisms that account for such delayed and morphologically different CPE in infected Calu-3

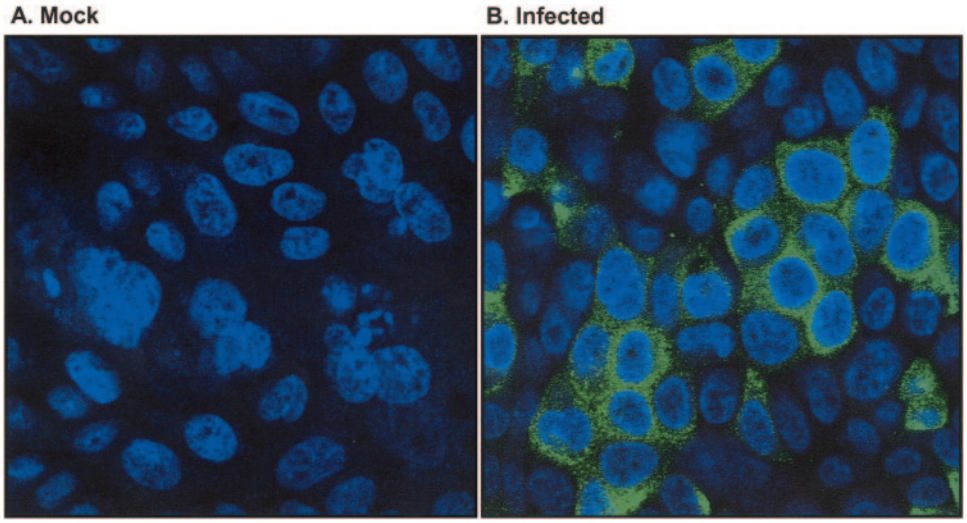

FIG. 3. Indirect immunofluorescence detection of SARS-CoV antigens in infected Calu-3 cells. Calu-3 monolayers grown on the chamber slides were mock infected or infected with SARS-CoV (MOI = 2). At 48 h after infection, nonpermeabilized Calu-3 cells were fixed with 2% paraformaldehyde and immunostained with a convalescent-phase serum from a SARS patient followed by a secondary FITC-conjugated goat anti-human IgG. Samples were examined by confocal microscopy. (A) Mock-infected monolayers showed only nuclear counterstain with DAPI. (B) SARS-CoV-specific antigens were readily detectable in clusters of infected Calu-3 monolayer.

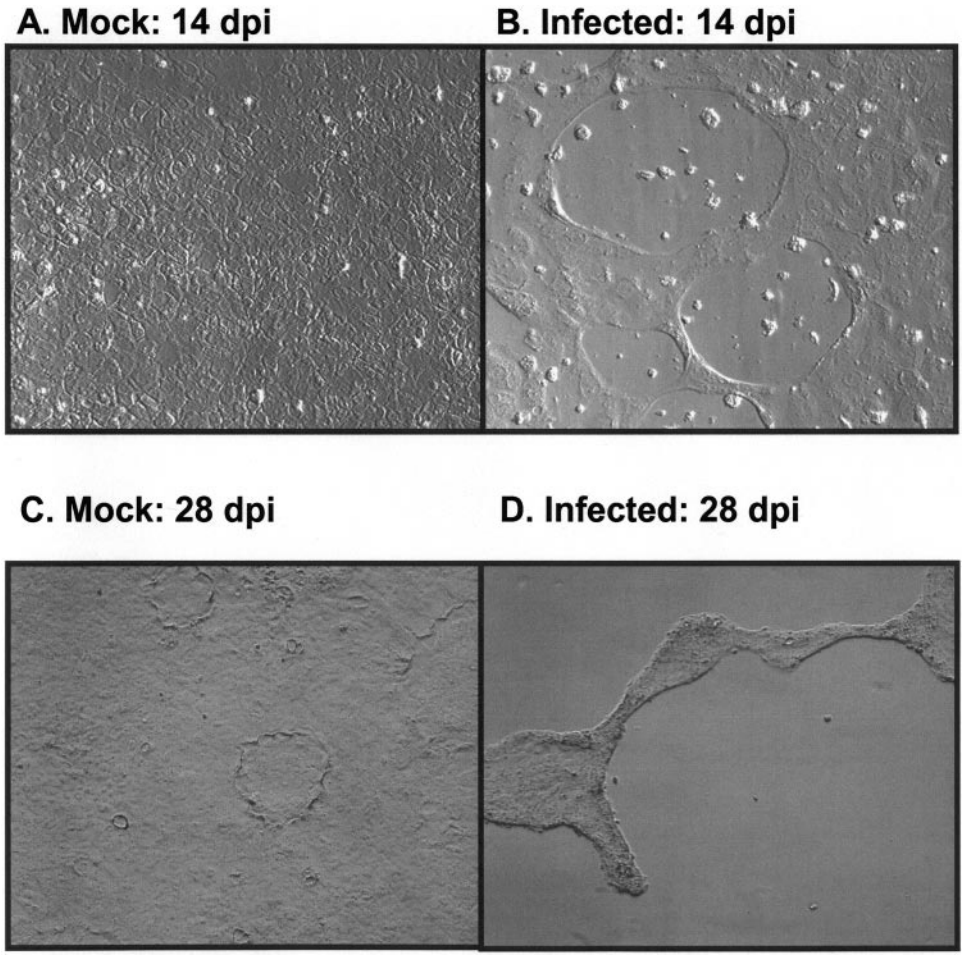

FIG. 4. SARS-CoV induces CPE on infected Calu-3 cells. Confluent Calu-3 cells were mock infected (A and C) or infected with SARS-CoV at an MOI of 1 (B and D) and cultured with DMEM medium containing 20% FCS. SARS-CoV-induced CPE was initially observed at day 8 after infection (not shown). The CPE at day 14 (B) and day 28 (D) after SARS-CoV infection were shown.

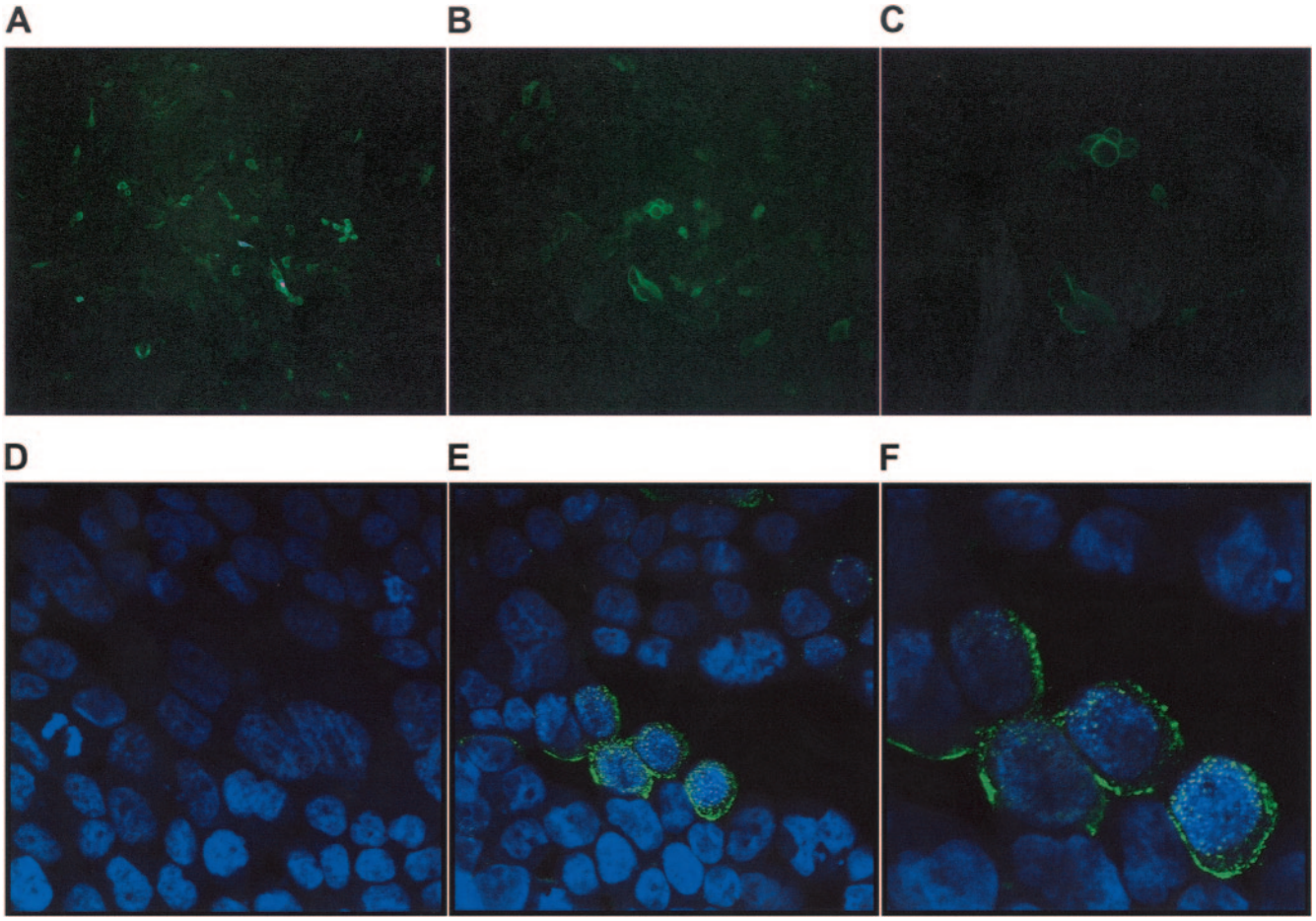

FIG. 5. Expression of the SARS-CoV receptor (ACE-2) on the surface of Calu-3 cells. Nonpermeabilized Calu-3 cells grown on the chamber slides were fixed with 2% paraformaldehyde and stained with goat anti-human ACE-2 plus FITC-conjugated rabbit anti-goat IgG and counterstained with DAPI for nucleus (blue). Stained samples were analyzed by both conventional fluorescence microscopy and confocal microscopy. (A to C) ACE-2 is expressed on the surface of a fraction of Calu-3 cells, as revealed by conventional microscopy. (E and F) Confocal images of ACE-2 expression on the surface of Calu-3 cells. When the primary antibody was substituted with normal goat serum, no signal of ACE-2 expression was detected (D). Data shown are representative of five independent experiments.

cells are currently unknown, the fact that SARS-CoV-induced CPE occurred considerably later than the maximal viral release suggests that a direct viral effect may not be responsible for cell death. Taken together, these results clearly demonstrate that human bronchial epithelial cells, as exemplified by Calu-3 here in this study, are susceptible to SARS-CoV infection. More significantly, the ability of SARS-CoV infection to induce CPE in Calu-3 cells appears to duplicate, to some degree, the histopathological manifestations in lung biopsies and autopsy specimens obtained from SARS patients (7, 22, 23, 30).

Expression of ACE-2 and its correlation with SARS-CoV infection in Calu-3 cells. A successful CoV infection starts with its interaction with specific cellular receptors (16). ACE-2 has recently been identified as a functional receptor for mediating SARS-CoV entry into permissive cells (20). Additionally, the induced expression of ACE-2 on nonpermissive cells via transfection with expressing plasmid often confers susceptibility to productive SARS-CoV infection (12, 33), indicating that ACE-2 alone is sufficient to allow viral entry. Thus, we initially investigated the expression of ACE-2 on Calu-3 cells by the flow cytometry using a goat anti-human ACE-2 polyclonal antibody and an FITC-conjugated secondary antibody. The FACS analysis revealed that approximately 30 to 70% of Calu-3 cells were positive for ACE-2 expression, depending on the gating (data not shown), with various staining intensity. We also used indirect immunofluorescence staining with a conventional immunofluorescence microscopy to localize the expression of ACE-2 in Calu-3 cells. As shown in Fig. 5A to C, the surface expression of ACE-2 could be detected in approximately 30% of Calu-3 cells by conventional immunofluorescence microscopy. At a higher magnification, clusters of cells that expressed ACE-2 on their surface could be readily visualized. The expression of ACE-2 on the surface of Calu-3 cells was also confirmed by studies with confocal microscopy. Figure 5D to F shows the clear demonstration of granular ACE-2 expression of different intensities on the surface of some, but not all, Calu-3 cells. The expression of ACE-2 in various tissues and cells has been extensively investigated with RT-PCR, Western blotting, immunohistochemistry, and flow cytometry (5, 11, 12, 20). To our knowledge, this is the first time that the surface expression of ACE-2 has been clearly demonstrated on the surface of cells permissive for SARS-CoV.

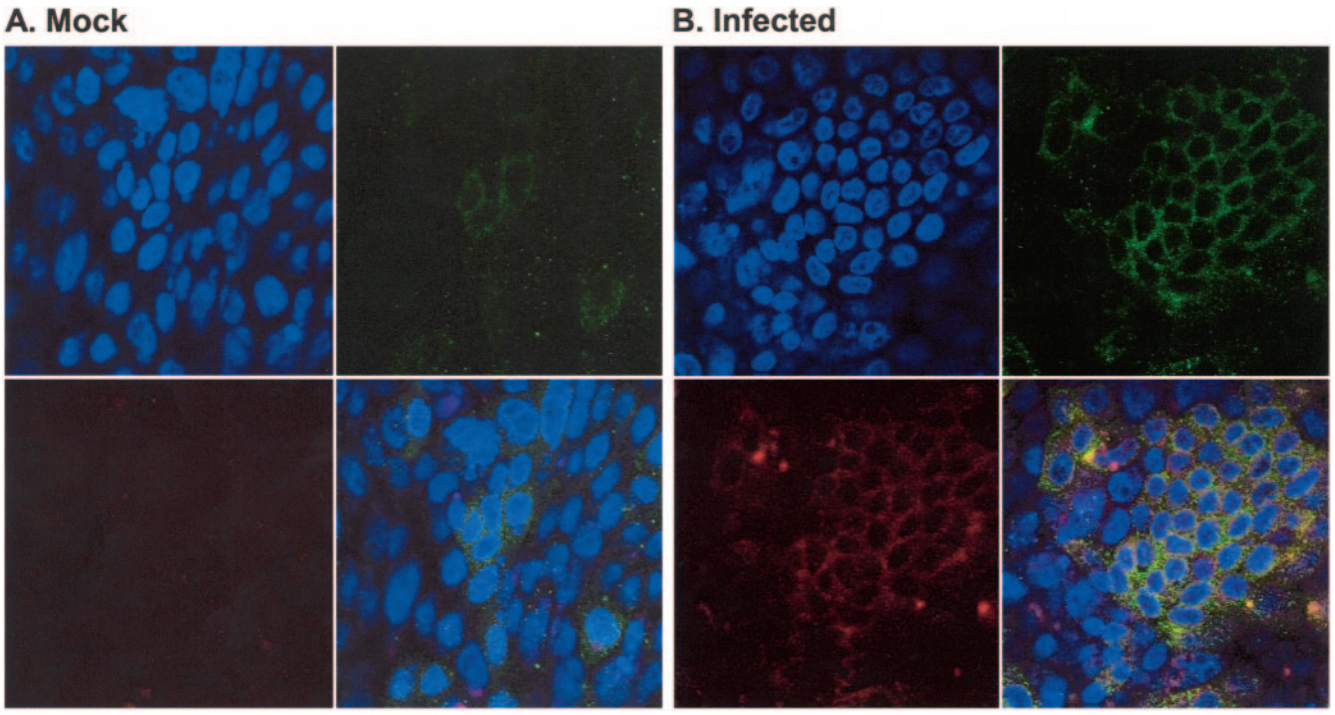

FIG. 6. Colocalization of ACE-2 and viral antigen in infected Calu-3 cells. Nonpermeabilized, mock-infected, and infected Calu-3 cells (MOI = 1) grown on the chamber slides were fixed with 2% paraformaldehyde at 48 h after infection. Uninfected and infected cells were stained with both goat anti-human ACE-2 antibody plus FITC-conjugated rabbit anti-goat IgG and rabbit anti-SARS-CoV NP antibody plus Texas red-conjugated donkey anti-rabbit IgG to detect the expression of ACE-2 (green) and SARS-CoV antigen (red). Samples were subjected to analysis with confocal microscopy. (A) Only ACE-2 signals could be detected in mock-infected cells; (B) both ACE-2 (green) and viral antigen (red) could be detected in infected cells. Importantly, both ACE-2 and viral antigen appeared to colocalize in infected cells (yellowish). Data shown are representative of four independent experiments.

The observation that only a fraction of Calu-3 cells was susceptible to SARS-CoV, as evidenced by the expression of viral antigens (Fig. 3), along with the demonstration of ACE-2 expression in some, but not all, Calu-3 cells (Fig. 5), prompted us to investigate the relationship between ACE-2 expression and SARS-CoV susceptibility of Calu-3 cells by two-color immunofluorescence staining. Uninfected and virally infected Calu-3 cells grown on the chamber slides were subjected to staining with pairs of goat anti-human ACE-2 antibody/FITC-conjugated rabbit anti-goat IgG and rabbit anti-SARS-CoV NP/Texas red-conjugated donkey anti-rabbit IgG. As shown in Fig. 6A and B, the expression of ACE-2 (green) was again restricted to some clusters of both uninfected and virally infected cells, whereas SARS-CoV-specific NP (red) could be detected only in a subset of cells infected with SARS-CoV for 2 days. Remarkably, a great majority of, if not all, Calu-3 cells showing the expression of viral antigen also coexpressed ACE-2 on their surface, as shown in the superimposed confocal imaging. Although studies of tissue and cellular distribution of ACE-2 have raised the possibility that ACE-2 may not be the only determinant of tissue and cellular tropism for SARS-CoV (5, 11), the highly colocalized expression of ACE-2 and viral antigen in infected Calu-3 cells strongly indicates that ACE-2 plays a central role in SARS-CoV infection.

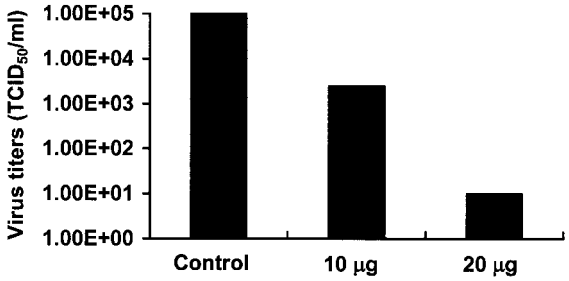

FIG. 7. Anti-ACE-2 antibody blocks the SARS-CoV replication in Calu-3 cells in a dose-dependent manner. Confluent Calu-3 cells grown in 96-well microtiter plates were treated with control goat antibody or goat anti-human ACE-2 antibody before infection with SARS-CoV at an MOI of 0.01. The resulting cell-free supernatants harvested at day 3 postinfection were subjected to the $TCID_{50}$ assays for quantifying the titers of infectious viruses. Data shown are representative of two independent experiments.

To further verify the role of ACE-2 in the viral replication, we treated Calu-3 cells with control antibody or various concentrations of anti-ACE-2 antibody before infection with SARS-CoV. The viral titer in supernatants harvested at day 3 after infection was determined. As shown in Fig. 7, addition of anti-ACE-2 antibody to the Calu-3 cell cultures resulted in a dose-dependent reduction of the infectious viral yields. Taken together, these results clearly demonstrate that the expression of ACE-2 is essential for SARS-CoV replication in Calu-3 cells.

SARS-CoV enters and is released from polarized Calu-3 cells preferentially through the apical membrane domain. The

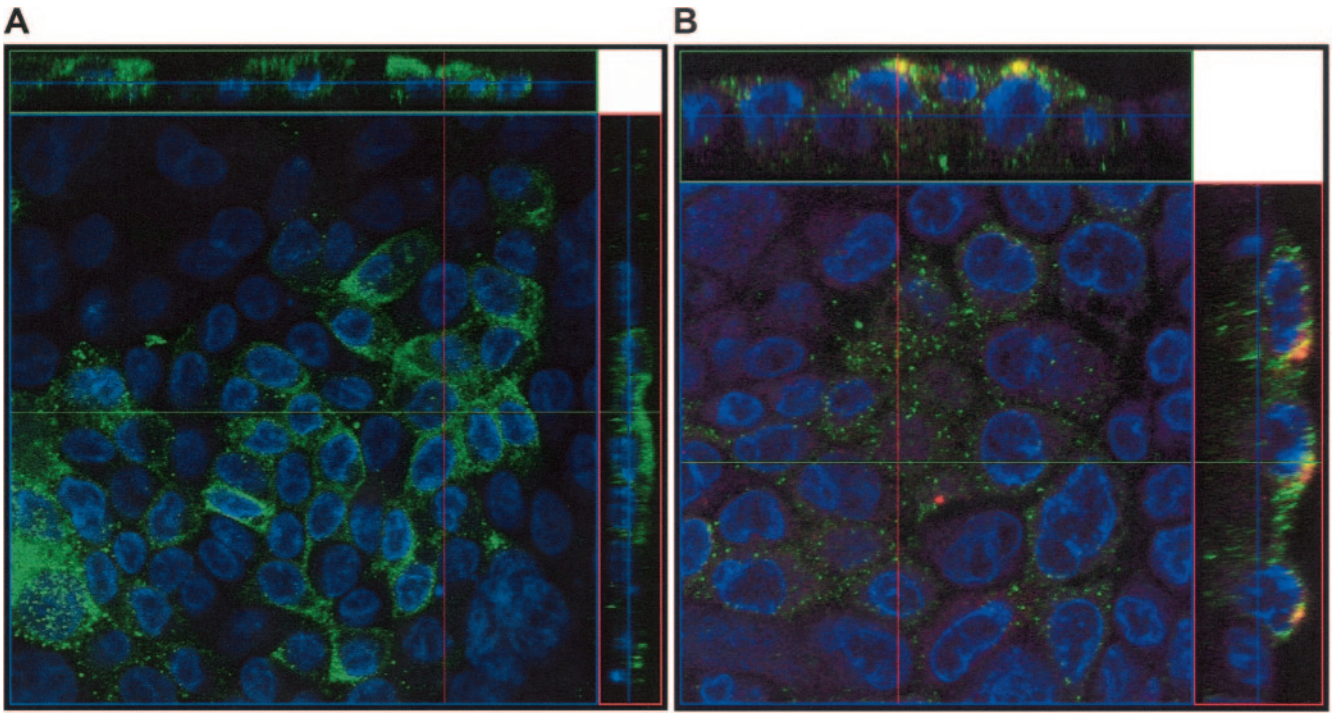

FIG. 8. Preferential colocalization of SARS-CoV antigens and ACE-2 at the apical surface of infected Calu-3 cells. Nonpermeabilized infected Calu-3 cells grown on the chamber slides were fixed with 2% paraformaldehyde at 48 h after infection and stained with a SARS convalescent-phase serum visualized by FITC-conjugated goat anti-human IgG alone (green [A]) or with both goat anti-human ACE-2 antibody plus FITC-conjugated rabbit anti-goat IgG (green [B]) and rabbit anti-SARS-CoV NP antibody plus Texas red-conjugated donkey anti-rabbit IgG (red [B]). Samples were examined by confocal microscopy. (A) SARS-CoV antigens (green) were detected in clusters of infected Calu-3 cells. Cross-*Z* section of the confocal imaging revealed a preferential viral antigen expression at the apical surface. (B) Confocal image (cross-*Z* section) of two-color staining showing colocalization of ACE-2 (Green) and SARS-CoV-specific NP antigen (red) at the apical surface of infected Calu-3 cells. Data shown are representative of two independent experiments.

pulmonary epithelial cell lining serves as a primary protective barrier against the entry of airborne respiratory pathogens. Plasma membranes of epithelial cells are highly polarized into two discrete domains (e.g., apical and basolateral membranes) that are separated by tight junctions that encircle the cells. The interaction of viruses with polarized epithelial cells has been extensively studied (31). Having shown that human bronchial epithelial Calu-3 cells were highly susceptible to SARS-CoV, we investigated the polarity of viral entry and release from

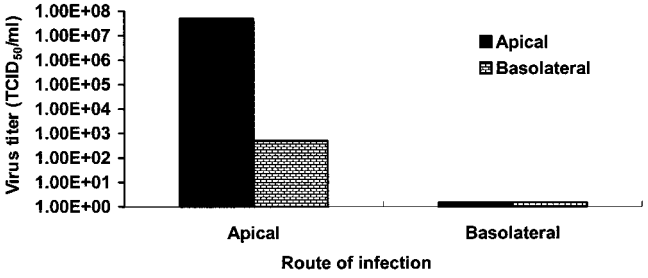

FIG. 9. Polarity of SARS-CoV entry and budding in Calu-3 cells. Polarized Calu-3 cells grown on filter inserts were inoculated with SARS-CoV (MOI = 1) through either the apical or basolateral surface. At 48 h after infection, the culture supernatants collected from the apical and basolateral chambers were assessed for the contents of infectious viral particles by the $TCID_{50}$ assay. The results are derived from a representative of two independently conducted experiments.

Calu-3 cells, aimed at understanding the role of pulmonary epithelial cells in respiratory SARS disease. We initially examined the expression of ACE-2 and viral antigens in infected Calu-3 cells grown on chamber slides using *Z* sections of confocal imaging, representing the longitudinal cross section of the infected monolayer. Fig. 8 shows the *Z*-section images of infected Calu-3 cells that have been immunostained with either an anti-SARS-CoV antibody alone or a combination of anti-ACE-2 and anti-SARS-CoV NP antibodies, as described above. Intense staining for SARS-CoV antigens (green) detected in infected cells was predominately restricted to the apical surface, with a very diffuse staining at the basolateral domain, as shown in Figure 8A. The expression of ACE-2 (green) correlated nicely with that of SARS-CoV-NP (red) at the apical surface of infected Calu-3 cells (Figure 8B). Thus, this polarized accumulation of viral antigens and/or ACE at the apical surface might suggest that SARS-CoV preferentially infects and/or is released from the apical surface of Calu-3 cells.

To further validate the polarity of SARS-CoV infection, Calu-3 cells were grown in filter inserts with a transwell system (Transwell-clear; Costar). Confluent Calu-3 monolayers were subjected to SARS-CoV infection at an MOI of 1 via either the apical or basolateral surfaces. At day 2 after infection, supernatants were collected from either the apical or basolateral chamber and assayed for infectious progeny virus, whereas the

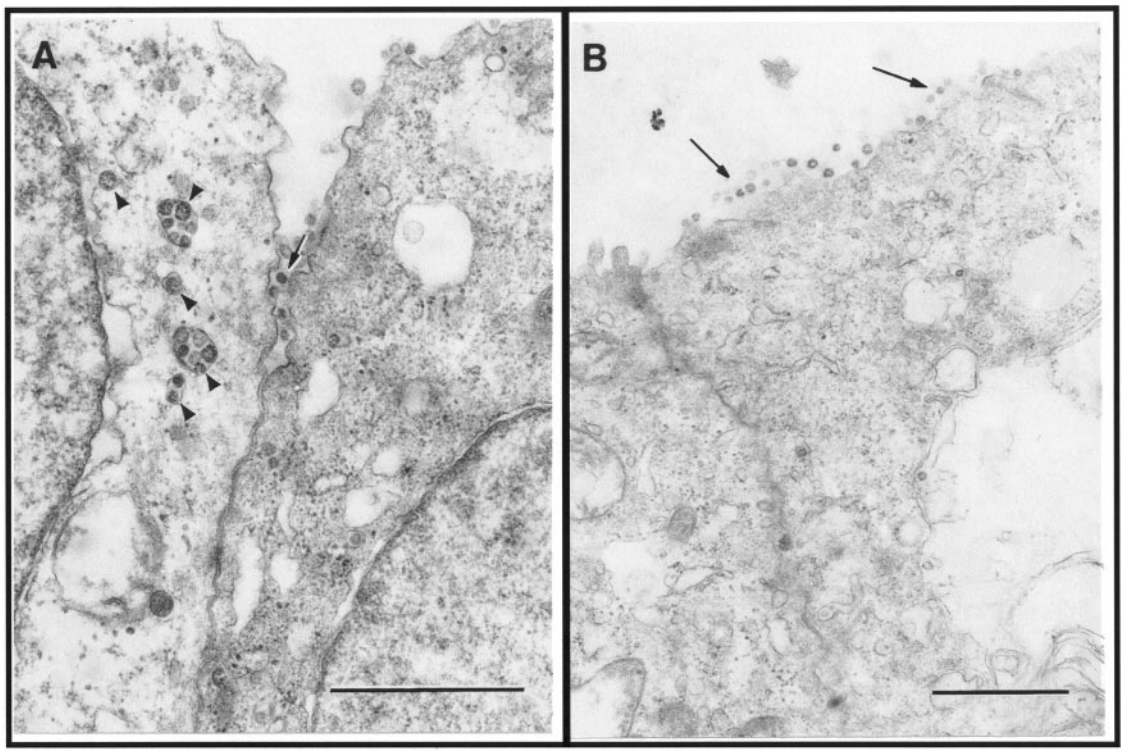

FIG. 10. Transmission electron microscopy of polarized Calu-3 cells infected with SARS-CoV. (A) Vesicles containing multiple viral particles (arrowheads) were frequently detected underneath the apical surface of polarized Calu-3 cells, but individual virions (arrow) were also detected at the apical junction of two polarized Calu-3 cells. (B) Release of SARS-CoV virions from the apical surface of polarized Calu-3 cells.

filter inserts containing infected monolayers were fixed and prepared for TEM. As shown in Fig. 9, infection through the apical surface resulted in the production of infectious progeny viruses, indicating the efficient entry of SARS-CoV into polarized Calu-3 cells through the apical surface. Strikingly, there was 5-log more infectious SARS-CoV particles recovered from the apical chamber than from the basolateral chamber of infected cultures, suggesting that the release of progeny SARS-CoV occurred almost exclusively via the apical membrane. The minute amounts of released virus present in the basolateral cultural medium may reflect either a limited basolateral release of virus from polarized cells or a leakage of the culture system, possibly due to the presence of a small number of incompletely polarized cells.

The preferential release of SARS-CoV from the apical surface was also demonstrated by TEM. As shown in Fig. 10, polarized Calu-3 cells were jointed to one another by typical tight junctions, and vesicles containing multiple nucleocapsids with electron-translucent and electron-dense cores can be seen aligned underneath the apical surface. Additionally, SARS-CoV particles present at the apical surface of a polarized epithelial cell and at the apical junction between two epithelial cells were also readily visible. Although a small proportion of released virus was also present in the basolateral chamber, attempts to localize viral particles at this domain by TEM were unsuccessful.

In contrast to the apical surface, infection through the basolateral surface of polarized cells did not result in the recovery of infectious viral particles from either chamber of the transwell system (Figure 9), suggesting that SARS-CoV may not properly interact with cells at the basolateral surface. Taken together, these results demonstrated that SARS-CoV efficiently infected polarized Calu-3 cells from the apical surface and also preferentially exited from the same surface.

A successful coronavirus infection of target cells relies heavily on its interaction with its cellular receptor (16). Thus, the preferential expression of ACE-2, a functional receptor for SARS-CoV, on the apical surface of Calu-3 cells, as shown in Figure 8, may provide a molecular basis for effective SARS-CoV infection through the apical membrane domain. It is possible that a critical receptor density may be a prerequisite for a successful SARS-CoV entry to succeed, and this receptor density may be present only on the apical surface. The insufficient expression of ACE-2 on the basolateral membrane domains may thus account for the unsuccessful SARS-CoV infection in polarized cells. Alternatively, the failure of SARS-CoV to basolaterally infect polarized cells could be due to the absence or insufficient expression of coreceptors, as indicated by recent reports (5, 11). These hypothetical coreceptors may be strictly polarized to the apical surface. Recently, CD209L (L-SIGN) was shown to be an additional receptor for SARS-CoV (14). It will be interesting to determine what additional role CD209L might have in mediating SARS-CoV entry into Calu-3 cells.

From our studies described above, the apical surface appears to be the primary site for SARS-CoV entry into and release from Calu-3 lung epithelial cells, a pattern shared by other respiratory viruses, including human CoV 229E, measles

virus, and human parainfluenza virus, interacting with polarized epithelial cells (2, 3, 32). Although the exact mechanism specifying this apical-surface-to-apical-surface entry and release of this virus is not clear, the polarized distribution of SARS-CoV receptor on the apical surface may be critically involved. This directional release of viral particles provides an excellent model for viral transmission and has interesting implications for viral pathogenesis; that is, when SARS-CoV is brought into contact with the airways via inhalation, it efficiently enters via the apical surface and replicates within bronchial epithelial cells. Once the replication is completed, the great majority of progeny viruses are released back into the lumen, where they could apically infect additional epithelial cells, be released back into the environment in respiratory droplets, or be taken up by alveolar MΦ, which may be ultimately responsible for taking the virus to the bloodstream. While most of the viruses are released into lumen via the apical surface, a small amount of basolaterally released progeny viruses might enter the circulation and propagate by infecting other non-respiratory-tract cells, including immune cells and intestinal epithelial cells, resulting in viremia and systemic infection. Moreover, we have recently shown that interactions of SARS-CoV with MΦ and dendritic cells (DC) can modulate various key functions of these two key innate cells, including phenotypic and functional maturation, phagocytosis, and inflammatory cytokine production (C. K. Tseng et al., unpublished data). Since SARS is believed to stem from an acute, profound, and unregulated inflammatory response in the lungs (7, 10, 17, 23, 30), active virus interactions with alveolar MΦ in the lumen and with DC that are dispersed between epithelial cells may be highly relevant to SARS pathogenesis. It is important that the polarity of SARS-CoV in our study was assessed at day 2 after infection, at which time no CPE could be observed. The fact that SARS-CoV infection eventually leads to the detachment of Calu-3 monolayers allows the argument that the strong apical polarization expected to dominate the earlier days of infection will be breached, thus enabling the virus to intimately interact with intraepithelial DC and other innate inflammatory cells.

In summary, we have characterized a SARS-CoV-susceptible epithelial cell line of human origin, Calu-3. We found that entry and release of SARS-CoV likely occurs at the apical surface in highly polarized Calu-3 cells. ACE-2, the receptor of SARS-CoV, is expressed predominately on the apical surface, which may play a crucial role in dictating viral infection. In contrast to other permissive human intestinal epithelial cell lines, with which SARS-CoV causes a persistent infection in the absence of CPE, Calu-3 cells respond to SARS-CoV by showing a delayed CPE, making it unique and potentially useful for studying the SARS-CoV-related pathogenesis of the respiratory system.

ACKNOWLEDGMENTS

We thank Li-Kung Chen from Tzu-Chi University at Hualien, Taiwan, and Tonya Eaves-Pyles at UTMB, Galveston, Tex., for kindly supplying convalescence serum from a SARS patient and the Calu-3 cell line, respectively; Vivian Braciale, Kui Li, and Shinji Makino for their critical review of the manuscript; Hongbing Zhu for her support with the tissue culture; and Mardelle Susman for her assistance with the submission of the manuscript.

This work was supported by the National Institutes of Health (NO1 AI 25489 to C.J.P.). J.T. was an undergraduate trainee from The University of Texas at Austin. L.P. is a predoctoral fellow of The James W. McLaughlin Foundation.

REFERENCES

1. **Basbaum, C. B., J. M. Madison, C. P. Sommerhoff, J. K. Brown, and W. E. Finkbeiner.** 1990. Receptors on airway gland cells. Am. Rev. Respir. Dis. **141:**S141–S144.
2. **Blau, D. M., and R. W. Compans.** 1995. Entry and release of measles virus are polarized in epithelial cells. Virology **210:**91–99.
3. **Bose, S., A. Malur, and A. K. Banerjee.** 2001. Polarity of human parainfluenza virus type 3 infection in polarized human lung epithelial A549 cells: role of microfilament and microtubule. J. Virol. **75:**1984–1989.
4. **Centers for Disease Control and Prevention.** 2003. Outbreak of severe acute respiratory syndrome—worldwide, 2003. Morb. Mortal. Wkly. Rep. **52:**226–228.
5. **Chan, P. K., K. F. To, A. W. Lo, J. L. Cheung, I. Chu, F. W. Au, J. H. Tong, J. S. Tam, J. J. Sung, and H. K. Ng.** 2004. Persistent infection of SARS coronavirus in colonic cells in vitro. J. Med. Virol. **74:**1–7.
6. **Chen, P. C., and C. H. Hsiao.** 2004. Re: to KF, Tong JH, Chan PK, et al. Tissue and cellular tropism of the coronavirus associated with severe acute respiratory syndrome: an in-situ hybridization study of fatal cases. J. Pathol 2004; 202: 157–163. J. Pathol. **203:**729–730.
7. **Ding, Y., H. Wang, H. Shen, Z. Li, J. Geng, H. Han, J. Cai, X. Li, W. Kang, D. Weng, Y. Lu, D. Wu, L. He, and K. Yao.** 2003. The clinical pathology of severe acute respiratory syndrome (SARS): a report from China. J. Pathol. **200:**282–289.
8. **Drosten, C., S. Gunther, W. Preiser, S. van der Werf, H. R. Brodt, S. Becker, H. Rabenau, M. Panning, L. Kolesnikova, R. A. Fouchier, A. Berger, A. M. Burguiere, J. Cinatl, M. Eickmann, N. Escriou, K. Grywna, S. Kramme, J. C. Manuguerra, S. Muller, V. Rickerts, M. Sturmer, S. Vieth, H. D. Klenk, A. D. Osterhaus, H. Schmitz, and H. W. Doerr.** 2003. Identification of a novel coronavirus in patients with severe acute respiratory syndrome. N. Engl. J. Med. **348:**1967–1976.
9. **Finkbeiner, W. E., S. D. Carrier, and C. E. Teresi.** 1993. Reverse transcription-polymerase chain reaction (RT-PCR) phenotypic analysis of cell cultures of human tracheal epithelium, tracheobronchial glands, and lung carcinomas. Am. J. Respir. Cell Mol. Biol. **9:**547–556.
10. **Franks, T. J., P. Y. Chong, P. Chui, J. R. Galvin, R. M. Lourens, A. H. Reid, E. Selbs, C. P. McEvoy, C. D. Hayden, J. Fukuoka, J. K. Taubenberger, and W. D. Travis.** 2003. Lung pathology of severe acute respiratory syndrome (SARS): a study of 8 autopsy cases from Singapore. Hum. Pathol. **34:**743–748.
11. **Hamming, I., W. Timens, M. L. Bulthuis, A. T. Lely, G. J. Navis, and H. van Goor.** 2004. Tissue distribution of ACE2 protein, the functional receptor for SARS coronavirus. A first step in understanding SARS pathogenesis. J. Pathol. **203:**631–637.
12. **Hofmann, H., K. Hattermann, A. Marzi, T. Gramberg, M. Geier, M. Krumbiegel, S. Kuate, K. Uberla, M. Niedrig, and S. Pohlmann.** 2004. S protein of severe acute respiratory syndrome-associated coronavirus mediates entry into hepatoma cell lines and is targeted by neutralizing antibodies in infected patients. J. Virol. **78:**6134–6142.
13. **Ikonen, E., and K. Simons.** 1998. Protein and lipid sorting from the trans-Golgi network to the plasma membrane in polarized cells. Semin. Cell Dev. Biol. **9:**503–509.
14. **Jeffers, S. A., S. M. Tusell, L. Gillim-Ross, E. M. Hemmila, J. E. Achenbach, G. J. Babcock, W. D. Thomas, Jr., L. B. Thackray, M. D. Young, R. J. Mason, D. M. Ambrosino, D. E. Wentworth, J. C. Demartini, and K. V. Holmes.** 2004. CD209L (L-SIGN) is a receptor for severe acute respiratory syndrome coronavirus. Proc. Natl. Acad. Sci. USA **101:**15748–15753.
15. **Ksiazek, T. G., D. Erdman, C. S. Goldsmith, S. R. Zaki, T. Peret, S. Emery, S. Tong, C. Urbani, J. A. Comer, W. Lim, P. E. Rollin, S. F. Dowell, A. E. Ling, C. D. Humphrey, W. J. Shieh, J. Guarner, C. D. Paddock, P. Rota, B. Fields, J. DeRisi, J. Y. Yang, N. Cox, J. M. Hughes, J. W. LeDuc, W. J. Bellini, and L. J. Anderson.** 2003. A novel coronavirus associated with severe acute respiratory syndrome. N. Engl. J. Med. **348:**1953–1966.
16. **Lai, M. M., and D. Cavanagh.** 1997. The molecular biology of coronaviruses. Adv. Virus Res. **48:**1–100.
17. **Lang, Z., L. Zhang, S. Zhang, X. Meng, J. Li, C. Song, L. Sun, and Y. Zhou.** 2003. Pathological study on severe acute respiratory syndrome. Chin. Med. J. **116:**976–980.
18. **Lee, N., D. Hui, A. Wu, P. Chan, P. Cameron, G. M. Joynt, A. Ahuja, M. Y. Yung, C. B. Leung, K. F. To, S. F. Lui, C. C. Szeto, S. Chung, and J. J. Sung.** 2003. A major outbreak of severe acute respiratory syndrome in Hong Kong. N. Engl. J. Med. **348:**1986–1994.
19. **Leung, G. M., A. J. Hedley, L. M. Ho, P. Chau, I. O. Wong, T. Q. Thach, A. C. Ghani, C. A. Donnelly, C. Fraser, S. Riley, N. M. Ferguson, R. M. Anderson, T. Tsang, P. Y. Leung, V. Wong, J. C. Chan, E. Tsui, S. V. Lo, and T. H. Lam.** 2004. The epidemiology of severe acute respiratory syndrome in the 2003

Hong Kong epidemic: an analysis of all 1755 patients. Ann. Intern. Med. **141:**662–673.
20. **Li, W., M. J. Moore, N. Vasilieva, J. Sui, S. K. Wong, M. A. Berne, M. Somasundaran, J. L. Sullivan, K. Luzuriaga, T. C. Greenough, H. Choe, and M. Farzan.** 2003. Angiotensin-converting enzyme 2 is a functional receptor for the SARS coronavirus. Nature **426:**450–454.
21. **Mossel, E., H. Cheng, K. Narayanan, R. Tesh, S. Makino, and C. Peters.** 2005. Exogenous ACE2 expression allows refractory cell lines to support severe acute respiratory syndrome coronavirus replication. J. Virol. **79:**3846–3850.
22. **Ng, M. L., S. H. Tan, E. E. See, E. E. Ooi, and A. E. Ling.** 2003. Early events of SARS coronavirus infection in Vero cells. J. Med. Virol. **71:**323–331.
23. **Nicholls, J. M., L. L. Poon, K. C. Lee, W. F. Ng, S. T. Lai, C. Y. Leung, C. M. Chu, P. K. Hui, K. L. Mak, W. Lim, K. W. Yan, K. H. Chan, N. C. Tsang, Y. Guan, K. Y. Yuen, and J. S. Peiris.** 2003. Lung pathology of fatal severe acute respiratory syndrome. Lancet **361:**1773–1778.
24. **Peiris, J. S., S. T. Lai, L. L. Poon, Y. Guan, L. Y. Yam, W. Lim, J. Nicholls, W. K. Yee, W. W. Yan, M. T. Cheung, V. C. Cheng, K. H. Chan, D. N. Tsang, R. W. Yung, T. K. Ng, and K. Y. Yuen.** 2003. Coronavirus as a possible cause of severe acute respiratory syndrome. Lancet **361:**1319–1325.
25. **Roberts, S. R., R. W. Compans, and G. W. Wertz.** 1995. Respiratory syncytial virus matures at the apical surfaces of polarized epithelial cells. J. Virol. **69:**2667–2673.
26. **Shen, B. Q., W. E. Finkbeiner, J. J. Wine, R. J. Mrsny, and J. H. Widdicombe.** 1994. Calu-3: a human airway epithelial cell line that shows cAMP-dependent Cl- secretion. Am. J. Physiol. **266:**L493–L501.
27. **Simmons, G., J. D. Reeves, A. J. Rennekamp, S. M. Amberg, A. J. Piefer, and P. Bates.** 2004. Characterization of severe acute respiratory syndrome-associated coronavirus (SARS-CoV) spike glycoprotein-mediated viral entry. Proc. Natl. Acad. Sci. USA **101:**4240–4245.
28. **Tashiro, M., M. Yamakawa, K. Tobita, J. T. Seto, H. D. Klenk, and R. Rott.** 1990. Altered budding site of a pantropic mutant of Sendai virus, F1-R, in polarized epithelial cells. J. Virol. **64:**4672–4677.
29. **Tsang, T., and T. H. Lam.** 2003. SARS: public health measures in Hong Kong. Respirology **8:**S46–S48.
30. **Tse, G. M., P. K. Hui, T. K. Ma, A. W. Lo, K. F. To, W. Y. Chan, L. T. Chow, and H. K. Ng.** 2004. Sputum cytology of patients with severe acute respiratory syndrome (SARS). J. Clin. Pathol. **57:**256–259.
31. **Tucker, S. P., and R. W. Compans.** 1993. Virus infection of polarized epithelial cells. Adv. Virus Res. **42:**187–247.
32. **Wang, G., C. Deering, M. Macke, J. Shao, R. Burns, D. M. Blau, K. V. Holmes, B. L. Davidson, S. Perlman, and P. B. McCray, Jr.** 2000. Human coronavirus 229E infects polarized airway epithelia from the apical surface. J. Virol. **74:**9234–9239.
33. **Wang, P., J. Chen, A. Zheng, Y. Nie, X. Shi, W. Wang, G. Wang, M. Luo, H. Liu, L. Tan, X. Song, Z. Wang, X. Yin, X. Qu, X. Wang, T. Qing, M. Ding, and H. Deng.** 2004. Expression cloning of functional receptor used by SARS coronavirus. Biochem. Biophys. Res. Commun. **315:**439–444.
34. **World Health Organization.** 2003. W.H.O. issues consensus document on the epidemiology of SARS. Wkly. Epidemiol. Rec. **78:**373–375.
35. **Zhan, J., W. Chen, C. Li, W. Wu, J. Li, S. Jiang, J. Wang, Z. Zeng, Z. Huang, and H. Huang.** 2003. Digestive system manifestations in patients with severe acute respiratory syndrome. Chin. Med. J. **116:**1265–1266.